



Preparation and performance of fluorescent polyacrylamide microspheres as a profile control and tracer agent

Wan-Li Kang^{1,2} · Lei-Lei Hu¹ · Xiang-Feng Zhang¹ · Run-Mei Yang¹ · Hai-Ming Fan¹ · Jie Geng¹

Received: 20 November 2014 / Published online: 24 July 2015
© The Author(s) 2015. This article is published with open access at Springerlink.com

Abstract Polyacrylamide microspheres have been successfully used to reduce water production in reservoirs, but it is impossible to distinguish polyacrylamide microspheres from polyacrylamide that is used to enhance oil recovery and is already present in production fluids. In order to detect polyacrylamide microspheres in the reservoir produced fluid, fluorescent polyacrylamide microspheres P(AM-BA-AMCO), which fluoresce under ultraviolet irradiation, were synthesized via an inverse suspension polymerization. In order to keep the particle size distribution in a narrow range, the synthesis conditions of the polymerization were studied, including the stirring speed and the concentrations of initiator, Na₂CO₃, and dispersant. The bonding characteristics of microspheres were determined by Fourier transform infrared spectroscopy. The surface morphology of these microspheres was observed under ultraviolet irradiation with an inverse fluorescence microscope. A laboratory evaluation test showed that the fluorescent polymer microspheres had good water swelling capability, thus they had the ability to plug and migrate in a sand pack. The plugging rate was 99.8 % and the residual resistance coefficient was 800 after microsphere treatment in the sand pack. Furthermore, the fluorescent microspheres and their fragments were accurately detected under ultraviolet irradiation in the produced fluid, even though they

had experienced extrusion and deformation in the sand pack.

Keywords Inverse suspension polymerization · Fluorescence · Polyacrylamide microsphere · Narrow size distribution · Profile control performance

1 Introduction

Polyacrylamide microspheres have been successfully applied to reduce water production and enhance oil recovery in mature reservoirs with well-developed fractures or ultra-high permeability streaks/channels (Yao et al. 2012, 2013; Hua et al. 2013; Li et al. 2014). However, it is impossible to distinguish polyacrylamide microspheres from polyacrylamide that was used to enhance oil recovery and was already present in production fluids.

Many inter-well tracers have been widely used to monitor the displacement into reservoirs and to obtain information on the interaction between producer and injector. These include chemical tracers (Wang et al. 2004b), nuclear tracers (Bjørnstad et al. 1990; Lien et al. 1988) and isotope tracers (Selby et al. 2007; Osborn and McIntosh 2010). However, some chemical tracers are easily absorbed onto the surface of rocks in the stratum, and the instruments required to detect radioactive isotopes are extremely expensive.

In recent years, fluorescence-detection technology has attracted great interest in oil field operations because of its convenience, high accuracy, and low cost. Wang et al. (2004a) used fluorescein as a tracer to monitor inter-well connectivity. Because the cost of the potassium iodide is ¥200,000 per year, and the cost of the fluorescein is only ¥15,000 per year. Yu et al. (2009) used fluorescein and

✉ Wan-Li Kang
kangwanli@126.com

¹ School of Petroleum Engineering, China University of Petroleum, Qingdao 266580, Shandong, China

² EOR Research Institute, China University of Petroleum (Beijing), Beijing 100249, China

calcein as inter-well tracers. The fluorescent method was simple and convenient with high precision and accuracy. The detection ranges for fluorescein and calcein were 0–0.35 and 0–0.89 mg/L, respectively, with a measurement error within 2.5 %. Yan et al. (2012) synthesized a fluorescent tracer copolymer (AM-AMCO) by emulsion polymerization of acrylamide and coumarin in the presence of $(\text{NH}_4)_2\text{S}_2\text{O}_8\text{-NaHSO}_3$ as a redox initiator. Characterization of the copolymer (AM-AMCO) indicated that fluorescent polyacrylamide can be used as an oilfield tracer and has good heat and salt resistance.

Coumarin, a benzopyrone, which has a large Stokes shift, high fluorescence quantum yield, and excellent light stability, is an attractive choice as a fluorescent candidate. Its derivatives have been widely used as fluorescent probes (Kalyanaraman et al. 2012), fluorescent indicator (Suzuki et al. 2002), and as fluorescent dye (Koops et al. 2010). In this study, 7-(allyloxy)-4-methyl-2H-chromen-2-one (AMCO), a derivative of coumarin, was selected as the fluorescent monomer grafted onto a water-soluble polymer to form fluorescent polyacrylamide microspheres.

Various methods can be used to synthesize polymer microspheres, such as emulsion polymerization (Chern 2006; Thickett and Gilbert 2007), soap-free emulsion polymerization (Nagao et al. 2006; Nakabayashi et al. 2013), dispersion polymerization (Covolan et al. 2000), precipitation polymerization (Chen et al. 2012; Bai et al. 2004), inverse-microemulsion polymerization (Hemingway et al. 2010), seeded polymerization (Zhang et al. 2011; Li et al. 2013), suspension polymerization (Liu et al. 2011; Zhao and Qiu. 2011), seeded dispersion polymerization (Tokuda et al. 2013), and inverse suspension polymerization (Annaka et al. 2003).

The inverse suspension polymerization method has many advantages. These are the heat of reaction is easily excluded from the reaction system; a granular product can be obtained directly without a crushing process; the product is easy to dry and has good water absorption performance. Recently, inverse suspension polymerization has broad application prospects in China (Guo et al. 2001; Tian et al. 2012). In order to obtain micron-sized microspheres with a narrow size distribution, inverse suspension polymerization was selected.

However, preparation conditions of the inverse suspension polymerization can affect the average particle size, and the average particle size will affect the profile control behavior of microspheres. Thus, the effect of preparation conditions on the average particle diameter needs to be discussed, including the stirring speed, the concentrations of initiator and dispersant.

In addition, the polyacrylamide microspheres cut excess water production by profile modification and blocking of paths with high permeability to water and enhance oil

recovery (EOR). So the swelling properties and the profile control performance of the fluorescent polyacrylamide microspheres were also investigated. As fluorescent polymer microspheres have the ability to fluoresce under ultraviolet irradiation; this can be widely used to detect the microspheres in the produced fluid.

2 Experimental

2.1 Materials

AMCO was synthesized by the method of Yan et al. (2012). Acrylamide (AM, a monomer), sorbitan monosuccinate (Span-60, an oil phase dispersant), anhydrous sodium carbonate (Na_2CO_3 , an electrolyte), *N, N'*-methylenebisacrylamide (MBA, a cross-linking agent), ammonium persulfate (APS, water-soluble initiator), cyclohexane (a continuous phase), anhydrous ethanol, and other reagents used were all of analytical-reagent grade and commercially available. The total salinity of the brine used was 6726 mg/L, and its main components are listed in Table 1. The brine viscosity was 1 mPa s.

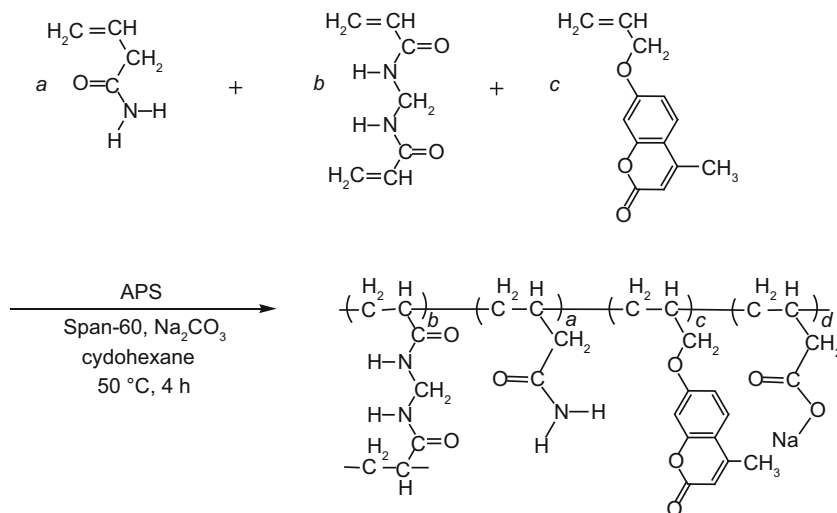
2.2 Methods

2.2.1 Synthesis and purification of fluorescent microspheres

Inverse suspension polymerization of fluorescent microspheres was carried out in a 250 mL four-neck flask. The flask was equipped with a mechanical stirrer, a reflux condenser, and a nitrogen inlet, and was incubated in a water bath. In inverse suspension polymerization, cyclohexane was used as a continuous phase and Span-60 as a nonionic polymeric surfactant. A synthesis route for fluorescent microspheres is shown in Scheme 1. Experimental procedures are as follows: (1) 0.07 g MBA, 14.06 g AM, and Na_2CO_3 were dissolved in 40 mL of distilled water. (2) This solution was then immediately poured into 60 mL of cyclohexane containing 0.014 g AMCO and Span-60, which was previously purged with dry nitrogen in the flask. (3) Air was flushed from the reactor by introducing nitrogen until the entire process was completed. (4) After aqueous droplets were observed in the continuous phase, 10 mL APS-water solution was added to the continuous phase to initiate polymerization. (5) Polymerization was allowed to proceed for 4 h at 50 °C. (6) Then stirring was stopped and the precipitate was washed with a large amount of methanol and filtered with qualitative filter paper (the pore size was about 1–3 μm). The product was dried in a vacuum oven at 45 °C for one day, and the obtained powder was fluorescent microspheres P(AM-BA-

Table 1 Brine components

Ion	K ⁺ + Na ⁺	Mg ²⁺	Ca ²⁺	Cl ⁻	SO ₄ ²⁻	HCO ₃ ⁻	CO ₃ ²⁻	Total salinity
Concentration, mg/L	2043	36	39	1337	10	3126	135	6726

**Scheme 1** Synthesis route of P(AM-BA-AMCO)

AMCO). The microspheres P(AM-BA) were prepared in the same way as above, without AMCO monomer in the reaction system.

2.2.2 Microsphere characterization

Fourier transform infrared spectroscopy (FTIR) spectra of P(AM-BA-AMCO), P(AM-BA), and acrylamide monomer were measured with a Nicolet model NEXUS670 spectrometer with samples prepared as KBr pellets. The surface morphology of the microspheres was observed in the DAPI fluorescence channel with an inverse fluorescence microscope (Leica DMI 3000B, Germany) at 25 °C.

The average particle size of microspheres, which is affected by different factors (i.e., stirring speed, concentrations of the initiator, dispersants, and Na₂CO₃) was determined at room temperature with a RISE-2006 laser particle size analyzer (Jinan Runzhi Technology Co., Ltd, China).

To measure the swelling ratio of microspheres, a tea bag (i.e., a 100 mesh nylon screen) containing pre-weighed dry samples was immersed entirely in the brine (with the composition given in Table 1). After being hydrated in brine for different times, the swollen microspheres were allowed to drain by removing the teabag from the brine and the excess surface water was removed with filter paper. The swelling ratio, S_w was calculated from the following equation:

$$S_w = (m_1 - m_0)/m_0, \quad (1)$$

where m_0 and m_1 are the weight of the dry and swollen microspheres, respectively.

2.2.3 Core flow experiment

Core flow experiments were designed to evaluate the effect of P(AM-BA-AMCO) on profile control. The core flow apparatus consisted of a constant-flux pump, a pressure sensor, and a sand pack ($d = 2.5$ cm, $L = 60$ cm, 20–50 mesh sand) (Fig. 1).

The core flow experiments were conducted conventionally at a flow rate of 5 mL/min at 45 °C. The sand pack was saturated with brine (1 PV) until the injection pressure stabilized. Then, 35 PV microsphere solution (2000 mg/L) was injected into the sand pack, followed by 25 PV brine. The differential pressures (ΔP , given in units of MPa) were measured during the whole injection process. The permeability of the sand pack in the displacement process (k , given in units of μm^2), and the plugging rate (η , expressed in units of %) were calculated using the following equations (Qin and Li 2006; Lei 2011):

$$k = \frac{Q\mu L}{10A\Delta P}, \quad (2)$$

$$\eta = \frac{k_0 - k'}{k_0} \times 100\%, \quad (3)$$

where Q is the injection rate, mL/s; μ the fluid viscosity, mPa s; L the length of the sand pack, cm; A is the sectional area of the sand pack, cm^2 , $A = \pi d^2/4$; ΔP is the

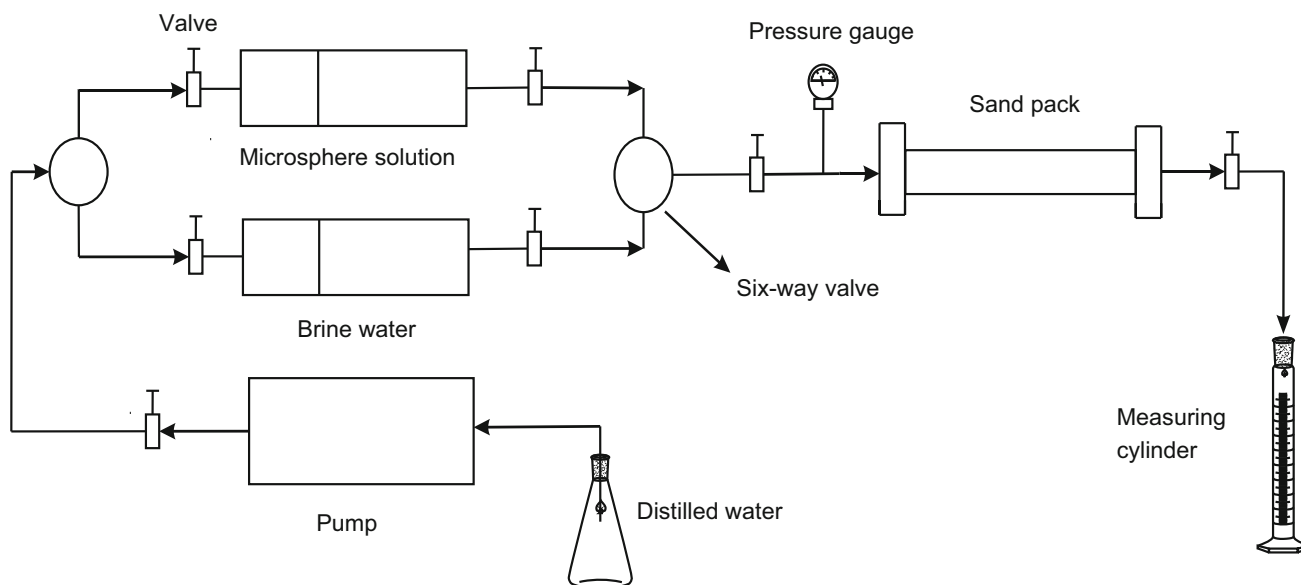


Fig. 1 Schematic illustration of the flow system

differential pressure, MPa; k_0 is the original permeability of the sand pack before microsphere treatment, μm^2 ; k' is the permeability of the sand pack after microsphere treatment, μm^2 .

The residual resistance factor, F_{rr} , is a measure of permeability reduction and is determined from laboratory data using the following equation:

$$F_{\text{rr}} = \frac{(\Delta P/Q)_{\text{after microsphere flow}}}{(\Delta P/Q)_{\text{before microsphere flow}}} \quad (4)$$

In this study the injection flow rate is kept constant before and after microsphere treatment, the Eq. (5) may be expressed as

$$F_{\text{rr}} = \frac{(\Delta P)_{\text{after microsphere flow}}}{(\Delta P)_{\text{before microsphere flow}}} \quad (5)$$

3 Results and discussion

3.1 FTIR spectrum of polyacrylamide microspheres

Figure 2 shows FTIR spectra of polyacrylamide microspheres and AM. A double peak at $3100\text{--}3500\text{ cm}^{-1}$ in the spectrum of AM, which is attributed to N–H stretching vibrations, disappeared in the spectra of P(AM-BA) and P(AM-BA-AMCO); whereas a peak at 3400 cm^{-1} , which is due to N–H stretching vibrations, was observed in the spectra of P(AM-BA) and P(AM-BA-AMCO). This indicates that acrylamide units exist within the structure of P(AM-BA) and P(AM-BA-AMCO). Furthermore, the C=O bending vibration was shifted

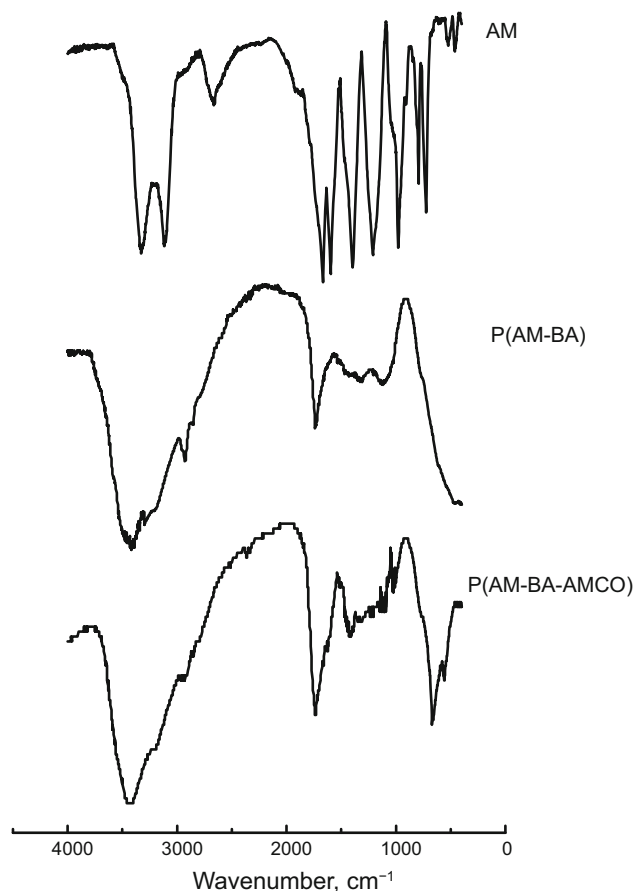


Fig. 2 A comparison of IR spectra of AM monomer, P(AM-BA), and P(AM-BA-AMCO)

from 1600 to 1740 cm^{-1} , which indicates that amide was partially hydrolyzed to carboxyl (Yang et al. 2007). A peak at 670 cm^{-1} is attributed to bending vibrations of aromatic hydrogen. The AMCO monomer which was connected to a side chain was at very low concentration. Therefore, other characteristic peaks of AMCO monomers are weak, such as from the benzene ring skeleton, methyl, and methylene.

3.2 Factors contributing to the average particle size of microspheres

We have found that with large amounts of monomers and high reaction temperature, bulk polymerization often took place in a very turbulent and even explosive form. It also has been found that a large amount of cross-linker could result in a reduction in swelling capability and mechanical toughness (Xia et al. 2003; Haraguchi et al. 2005). Therefore, the effect of reaction temperature and the concentrations of AM, MBA monomers were not investigated in this work.

3.2.1 Stirring speed

Figure 3a shows the effect of stirring speed on the average particle size of microspheres. The average particle size of

microspheres decreased from 260 to 125 μm when the stirring speed increased from 150 to 300 r/min, but when the stirring speed increased from 300 to 500 r/min, the average particle size of microspheres increased greatly. At low stirring speeds (<300 r/min), big droplets are broken down and dispersed due to stirring, and the average particle size becomes smaller as a result. However, at high stirring speeds (300–500 r/min), the possibility of collisions between droplets is increased, which results in an increase in the average particle size. Besides, high stirring speeds would destroy the structure of microspheres, and would increase the particle size distribution of the microspheres. So, we set the mechanically stirring speed at 300 r/min in order to obtain an average particle size of 125 μm and to keep the particle size distribution in a narrow range.

3.2.2 Initiator (APS) concentration

The effect of APS concentration on the average particle size of microspheres is shown in Fig. 3b. The plot shows that with an increase in the APS concentration, the average particle size of microspheres increased significantly. This might be because, as the APS concentration increases, free radicals derived primarily from initiator (APS) increase within the time tested. Under the assumptions that each

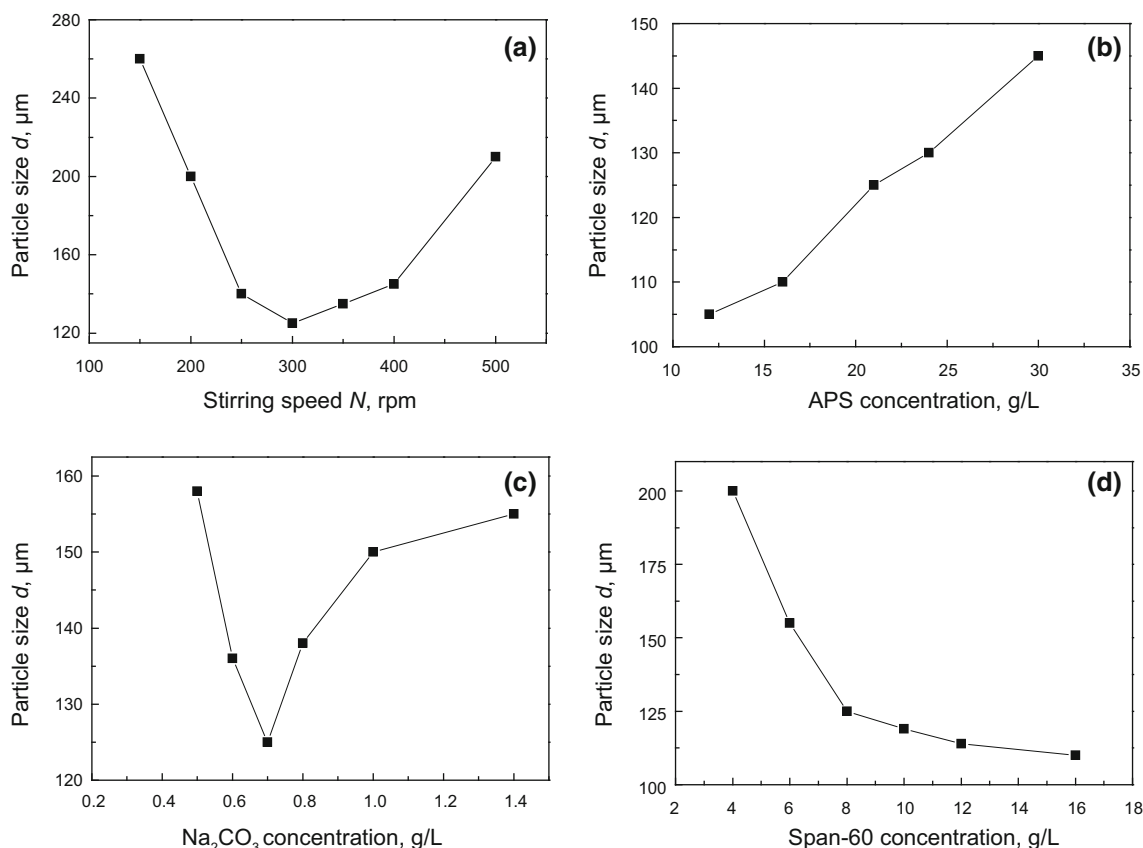


Fig. 3 Factors contributing to the average particle size. **a** Stirring speed; **b** APS concentration; **c** Na_2CO_3 concentration; **d** Span-60 concentration

polymer chain growth rate is same, this increase in free radicals results in a reduction in the relative molecular mass of the polymer, and a consequent increase in the polymer solubility in the aqueous phase. In order to generate microspheres of small average particle size, the APS concentration should be controlled between 20.0–24.0 g/L.

3.2.3 Na_2CO_3 concentration

Figure 3c shows that the average particle size of microspheres is reduced from 158 to 125 μm as the Na_2CO_3 concentration increased from 0.5 to 0.7 g/L. However, when the Na_2CO_3 concentration is increased from 0.7 to 1.4 g/L, the average particle size increased from 125 to 155 μm gradually.

First of all, APS as an initiator is decomposed into fragments and then adsorbs around the droplets to form electrical double layers, which must give rise to repulsion forces whenever two droplets approach each other to maintain the stability of droplets (this is the fundamental factor responsible for the stability of droplets). Secondly, the added Na_2CO_3 increases the ionic strength of the system, so the electric double layers formed at the droplet surfaces become thinner. Therefore, the electrostatic repulsion between droplets reduces, which increases the probability of initial intergranular coalescence, with the result that the average particle size of microspheres increases.

3.2.4 Dispersant (Span-60) concentration

Smaller microspheres may be produced by increasing the dispersant concentration. Figure 3d shows that with an increase in the Span-60 concentration from 4 to 16 g/L, the average particle size decreased gradually from 200 to 110 μm . This might be because the dispersants adsorbed onto the droplet surface obstruct the agglomeration between droplets.

In order to obtain relatively uniform fluorescent microspheres of an average particle size about 120 μm , the dispersant concentration (Span-60) should be kept at 8–10 g/L.

3.3 Size distribution of microspheres

When the weights of AM, MBA, AMCO were 14.06, 0.07, 0.014 g, the concentration of the APS, Na_2CO_3 , Span-60 were 2, 0.7, 8 g/L, respectively, and the stirring speed was 300 r/min, the microspheres were obtained with a narrow size distribution. Figure 4 shows an optical micrograph and particle size distribution of microspheres in ethanol at 25 °C. It can be seen that the particle size of microspheres was 120–130 μm , with an average particle size of 125 μm .

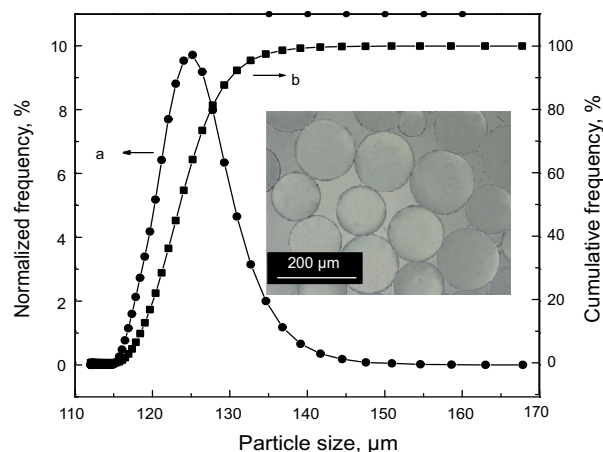


Fig. 4 Particle size distribution of elastic microspheres in ethanol at 25 °C

3.4 The swelling properties of microspheres

Figure 5 shows the swelling ratio of microspheres after being hydrated in brine. Within 24 h of hydration, the swelling ratio increased significantly to about 10 and gradually leveled off until 180 h, which indicates that brine can penetrate into the microsphere matrix. In fact, the microspheres are cross-linked particles with a three-dimensional network structure and many free hydrophilic groups ($-\text{CONH}_2$) inside. Polar water molecules can bond with these groups easily through hydrogen bonding and cause a significant increase in the size of the hydrated microspheres.

Furthermore, swelling behavior of P(AM-BA-AMCO) microspheres is similar to P(AM-BA) microspheres. This indicates that the swelling property of P(AM-BA-AMCO) has not been dramatically affected by the fluorescent group

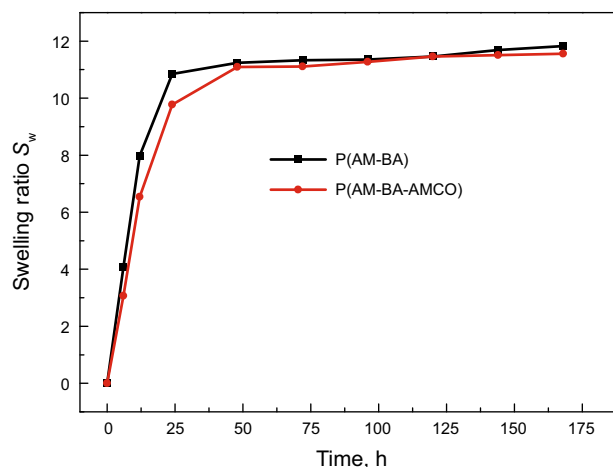


Fig. 5 Swelling properties of microspheres in brine at 45 °C

due to a low content of fluorescent group embedded in microspheres by grafting or coating.

3.5 Profile control performance of microspheres

The pressure drop during the core flow experiments was used to calculate residual resistance factor (F_{rr}) and the differential pressure was monitored, shown in Fig. 6. The differential pressure rose from around 1 kPa (stabilized pressure at the end of water flood) to around 1.8 MPa with the injection of the microsphere solution (0–35 PV). After 35 PV of microsphere injection, brine was injected into the sand pack. The differential pressure quickly dropped down to about 0.9 MPa (35–36 PV) thereafter gently drop at the range of 35–63 PV, and finally leveled off around 0.8 MPa.

The differential pressure fluctuates within a wide range at the second-stage (II), and this phenomenon was defined as “wave-type variation” (Yao et al. 2012). In the subsequent injection of brine, the pressure remains in this kind of variation in the range of 35–60 PV and then reaches a relatively high and constant level. In fact, when the brine-swelled microspheres were injected into the sand pack, they first adsorbed and accumulated near the inlet of the sand pack, causing the differential pressure to increase. Moreover, with the increased injection volume of microspheres, microspheres accumulated more and more, making the pressure rise faster. The differential pressure increased and fluctuated during the microsphere treatment stage (II) and the subsequent water flooding stage (III). This phenomenon indicates that the swelled microspheres have a certain degree of deformation ability and could deform under pressure to advance into the sand pack, to play the role of profile modification (Hua et al. 2013).

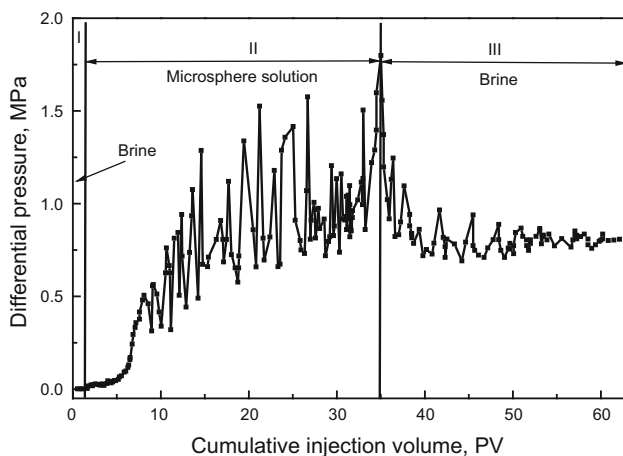


Fig. 6 Relationship between the differential pressure and injection volume

It can be inferred from Table 2 that at first brine could be injected into the sand pack at a relatively low pressure (1 kPa) due to high initial permeability of sand pack ($102 \mu\text{m}^2$). After injection of 1.0 PV brine and 35 PV microsphere solution, the sand pack permeability decreased to $0.06 \mu\text{m}^2$, while the resultant differential pressure increased to 1.8 MPa. In the subsequent injection of brine, the sand pack permeability was restored to $0.13 \mu\text{m}^2$ and the differential pressure was restored to 0.8 MPa. Meanwhile, the plugging rate was 99.8 % and the residual resistance factor was 800. This indicates that the microspheres injected into the sand pack would swell several times and deposit in pores and throats in the high-permeability unconsolidated sand packs, resulting in a reduction in permeability and an increase in residual resistance factor.

3.6 Surface morphology of P(AM-BA-AMCO) microspheres

The surface topography of P(AM-BA-AMCO) microspheres was observed with the inverse fluorescence microscope and shown in Fig. 7. The phase-contrast images of Fig. 7a, c was taken under natural light. Figure 7b, d was taken under ultraviolet irradiation. Fluorescent microspheres were spheroid-shaped, with a smooth surface and an average diameter of about $200 \mu\text{m}$. Furthermore, fluorescence microscopy images demonstrated that the fluorescent monomers were uniformly distributed inside the microspheres and they had kept their fluorescent properties after swelling.

Figure 7c, d shows the images of P(AM-BA-AMCO) microspheres come out from the outlet of the unconsolidated sand pack after the subsequent water flooding experiment. It can be seen that the P(AM-BA-AMCO) microspheres and their fragments were accurately detected in the produced fluid. Such microspheres and fragments still released blue fluorescence under ultraviolet irradiation, even though they have experienced extrusion and deformation in the sand pack. These P(AM-BA-AMCO) microspheres may be potentially distinguished from the reservoir produced fluid.

4 Conclusions

- (1) Coumarin fluorescent polyacrylamide microspheres [P(AM-BA-AMCO)], with an average particle size of $125 \mu\text{m}$, were synthesized with the inverse suspension polymerization method.
- (2) The microspheres had the ability to plug fractures and pores in the sand pack. The plugging rate was

Table 2 Changes in core permeability and injection pressure in plug process

Permeability, μm^2			Differential pressure, MPa			Plugging rate, %	Residual resistance factor F_{rr}
Initial	At 35 PV	At 63 PV	Initial	At 35 PV	At 63 PV		
102	0.06 ^a	0.13	0.001	1.8	0.8	99.8	800

^a Permeability to water. The viscosity of the microsphere solution is 1 mPa s

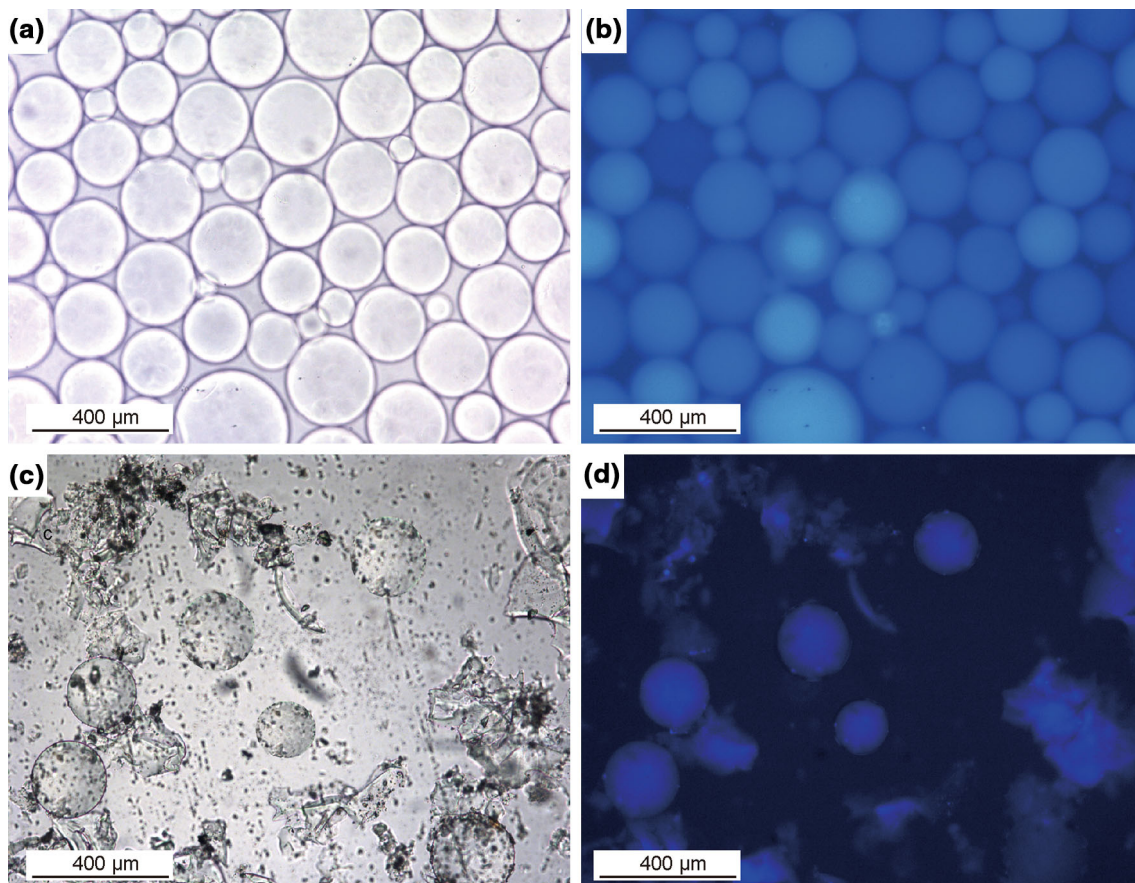


Fig. 7 Fluorescence microscope images of P(AM-BA-AMCO) microspheres. **a** Phase-contrast image of microspheres under the natural light after swelling for 24 h in brine; **b** Fluorescence micrographs for the (a) taken under ultraviolet irradiation; **c** Phase-contrast image of microspheres under the natural light which came out from the outlet of the unconsolidated sand pack after the subsequent water flooding experiment; **d** Fluorescence micrographs for the (c) taken under ultraviolet irradiation

99.8 % and the residual resistance factor was 800 after microsphere treatment.

- (3) The microspheres and their fragments could be accurately detected in the produced fluid even though they experienced extrusion and deformation in the sand pack. This is a potential application value of fluorescent microspheres, and can be used to detect the polyacrylamide microspheres in produced liquid.

Acknowledgments This research was supported by the National Natural Science Foundation of China (No. 21273286), Doctoral Program Foundation of the Education Ministry (No. 20130133110005).

Open Access This article is distributed under the terms of the Creative Commons Attribution 4.0 International License (<http://creativecommons.org/licenses/by/4.0/>), which permits unrestricted use, distribution, and reproduction in any medium, provided you give appropriate credit to the original author(s) and the source, provide a link to the Creative Commons license, and indicate if changes were made.

References

- Annaka M, Matsuura T, Kasai M, et al. Preparation of comb-type *N*-isopropylacrylamide hydrogel beads and their application for size-selective separation media. *Biomacromolecules*. 2003;4(2):395–403.
- Bai F, Yang XL, Huang WQ. Synthesis of narrow or monodisperse poly(divinylbenzene) microspheres by distillation-precipitation polymerization. *Macromolecules*. 2004;37(26):9746–52.
- Bjørnstad T, Brendsdal E, Michelsen OB, et al. Analysis of radiolabelled thiocyanate tracer in oil field brines. *Nucl Instrum Methods Phys Res, Sect A*. 1990;299:629–33.
- Chen Y, Tong LY, Zhang D, et al. Thermostable microspheres consisting of poly(*N*-phenylmaleimide-co- α -methyl styrene) prepared by precipitation polymerization. *Ind Eng Chem Res*. 2012;51:15610–7.
- Chern CS. Emulsion polymerization mechanisms and kinetics. *Prog Polym Sci*. 2006;31(5):443–86.
- Covolan VL, D'Antone S, Ruggeri G, et al. Preparation of aminated polystyrene latexes by dispersion polymerization. *Macromolecules*. 2000;33(18):6685–92.
- Guo JW, Cui YD, Kang Z, et al. Synthesis of superabsorbent polymers by the inverse suspension method. *Fine Chem*. 2001;18(6):348–50 (in Chinese).
- Haraguchi K, Li HJ, Matsuda K, et al. Mechanism of forming organic/inorganic network structures during in situ free-radical polymerization in PNIPA-clay nanocomposite hydrogels. *Macromolecules*. 2005;38(8):3482–90.
- Hemingway MG, Gupta RB, Elton DJ. Hydrogel nanopowder production by inverse-mini-emulsion polymerization and supercritical drying. *Ind Eng Chem Res*. 2010;49(20):10094–9.
- Hua Z, Lin MQ, Guo JR, et al. Study on plugging performance of cross-linked polymer microspheres with reservoir pores. *J Petrol Sci Eng*. 2013;105:70–5.
- Kalyanaraman B, Darley-Usmar V, Davies KJA, et al. Measuring reactive oxygen and nitrogen species with fluorescent probes: challenges and limitations. *Free Radical Biol Med*. 2012;52(1):1–6.
- Koops SE, Barnes PRF, O'Regan BC, et al. Kinetic competition in a coumarin dye-sensitized solar cell: injection and recombination limitations upon device performance. *J Phys Chem C*. 2010;114(17):8054–61.
- Lei GL. New deep profile control and flooding technology using pore-scale elastic microspheres. Dongying: China University of Petroleum Press; 2011 (in Chinese).
- Li BX, Xu YF, Wang MZ, et al. Morphological control of multihollow polymer latex particles through a controlled phase separation in the seeded emulsion polymerization. *Langmuir*. 2013;29(48):14787–94.
- Li JJ, Liu YZ, Na Z, et al. Investigation on the adaptability of the polymer microspheres for fluid flow diversion in porous media. *J Dispers Sci Technol*. 2014;35(1):120–9.
- Lien JR, Graue A, Kolltveit K. A nuclear imaging technique for studying multiphase flow in a porous medium at oil reservoir conditions. *Nucl Instrum Methods Phys Res, Sect A*. 1988;3:693–700.
- Liu ZD, Lu YC, Yang BD, et al. Controllable preparation of poly(butyl acrylate) by suspension polymerization in a coaxial capillary microreactor. *Ind Eng Chem Res*. 2011;50(21):11853–62.
- Nagao D, Sakamoto T, Konno H, et al. Preparation of micrometer-sized polymer particles with control of initiator dissociation during soap-free emulsion polymerization. *Langmuir*. 2006;22(26):10958–62.
- Nakabayashi K, Kojima M, Inagi S, et al. Size-controlled synthesis of polymer nanoparticles with tandem acoustic emulsification followed by soap-free emulsion polymerization. *ACS Macro Lett*. 2013;2:482–4.
- Osborn SG, McIntosh JC. Chemical and isotopic tracers of the contribution of microbial gas in Devonian organic-rich shales and reservoir sandstones, northern Appalachian Basin. *Appl Geochem*. 2010;25(3):456–71.
- Qin JS, Li AF. Reservoir physics. Dongying: China University of Petroleum Press; 2006 (in Chinese).
- Selby D, Creaser RA, Fowler MG. Re-Os elemental and isotopic systematics in crude oils. *Geochim Cosmochim Acta*. 2007;71(2):378–86.
- Suzuki Y, Komatsu H, Ikeda T, et al. Design and synthesis of Mg²⁺-selective fluoroionophores based on a coumarin derivative and application for Mg²⁺ measurement in a living cell. *Anal Chem*. 2002;74(6):1423–8.
- Thickett SC, Gilbert RG. Emulsion polymerization: state of the art in kinetics and mechanisms. *Polymer*. 2007;48(24):6965–91.
- Tian JJ, Ma F, Yu XL, et al. Technology process investigation of superabsorbent resin by inverse suspension polymerization. *J Wuhan Inst Tech*. 2012;34(11):9–13 (in Chinese).
- Tokuda M, Shindo T, Minami H. Preparation of polymer/poly(ionic liquid) composite particles by seeded dispersion polymerization. *Langmuir*. 2013;29(36):11284–9.
- Wang BJ, Guo MR, Lv KF, et al. The application of fluorescein as an oil field tracer. Chinese patent: CN1415978A. 2004a (in Chinese).
- Wang TG, He FJ, Li MJ, et al. Alkyldibenzothiophenes: molecular tracers for filling pathway in oil reservoirs. *Chin Sci Bull*. 2004b;49(22):2399–404.
- Xia XH, Yih J, D'Souza NA, et al. Swelling and mechanical behavior of poly (*N*-isopropylacrylamide)/Na-montmorillonite layered silicates composite gels. *Polymer*. 2003;44(16):3389–93.
- Yan LW, Peng CX, Ye ZB, et al. Synthesis and evaluation of a water-soluble copolymer (AM-AMCO) as a fluorescent tracer. *Chem Res Appl*. 2012;24(6):996–1001 (in Chinese).
- Yang WB, Xia MF, Li AM, et al. Mechanism and behavior of surfactant adsorption onto resins with different matrices. *React Funct Polym*. 2007;67(7):609–16.
- Yao CJ, Lei GL, Li L, et al. Selectivity of pore-scale elastic microspheres as a novel profile control and oil displacement agent. *Energy Fuels*. 2012;26(8):5092–101.
- Yao CJ, Lei GL, Cheng MM. A novel enhanced oil recovery technology using pore-scale elastic microspheres after polymer flooding. *Res J Appl Sci Eng Technol*. 2013;6(19):3634–7.
- Yu JT, Wang LY, Wang H, et al. Determination of interwell tracers by fluorospectrophotometry. *Chem Ind Eng*. 2009;26(3):256–61 (in Chinese).
- Zhang MC, Lan Y, Wang D, et al. Synthesis of polymeric Yolk-Shell microspheres by seed emulsion polymerization. *Macromolecules*. 2011;44(4):842–7.
- Zhao T, Qiu D. One-pot synthesis of highly folded microparticles by suspension polymerization. *Langmuir*. 2011;27(21):12771–4.